13. L. A. Posey, R. D. Guettler, N. J. Kirchner, R. N. Zare, *ibid.* **101**, 3772 (1994).
14. W. E. Conaway, R. J. S. Morrison, R. N. Zare, *Chem. Phys. Lett.* **113**, 429 (1985).
15. P. J. Miller, S. D. Colson, W. A. Chupka, *ibid.* **145**, 183 (1988).
16. M. N. R. Ashfold, C. L. Bennett, R. J. Stickland, *Comments At. Mol. Phys.* **19**, 181 (1987).
17. W. R. Harshbarger, *J. Chem. Phys.* **53**, 903 (1970).
18. D. J. Leahy and R. N. Zare, unpublished data.
19. R. D. Guettler *et al.*, *J. Chem. Phys.* **101**, 3763 (1994).
20. J. H. Glownia, S. J. Riley, S. D. Colson, J. C. Miller, R. N. Compton, *ibid.* **77**, 68 (1982).
21. J. B. Pallix and S. D. Colson, *J. Phys. Chem.* **90**, 1499 (1986).
22. S. Tomoda, S. Suzuki, I. Koyano, *J. Chem. Phys.* **89**, 7268 (1988).
23. W. J. Chesnavich and M. T. Bowers, *Chem. Phys. Lett.* **52**, 179 (1977).
24. W. E. Conaway, T. Ebata, R. N. Zare, *J. Chem. Phys.* **87**, 3453 (1987).
25. W. A. Chupka and M. E. Russell, *ibid.* **48**, 1527 (1968).
26. T. Baer and P. T. Murray, *ibid.* **75**, 4477 (1981).
27. D. V. Pijkeren, E. Boltjes, J. V. Eck, A. Niehaus, *Chem. Phys.* **91**, 293 (1984).
28. H. Tachikawa and S. Tomoda, *ibid.* **182**, 185 (1994).
29. L.A.P. was supported by an NSF Postdoctoral Research Fellowship in Chemistry (CHE-89-07493). Financial support also came from the Air Force Office of Scientific Research (F49620-92-J-0074).

24 June 1994; accepted 2 August 1994

Spring Phytoplankton Production in the Western Ross Sea

Kevin R. Arrigo* and Charles R. McClain

Coastal zone color scanner (CZCS) imagery of the western Ross Sea revealed the presence of an intense phytoplankton bloom covering >106,000 square kilometers in early December 1978. This bloom developed inside the Ross Sea polynya, within 2 weeks of initial polynya formation in late November. Primary productivity calculated from December imagery (3.9 grams of carbon per square meter per day) was up to four times the values measured during in situ studies in mid-January to February 1979. Inclusion of this early season production yields a spring-to-summer estimate of 141 to 171 grams of carbon per square meter, three to four times the values previously reported for the western Ross Sea.

In the western Ross Sea (Fig. 1), a large polynya forms north of the Ross Ice Shelf in late spring. The availability of light and nutrients within this polynya favors algal growth, and blooms of phytoplankton (pigment >1 mg m^{-3}) have been observed there in mid-January and later (*1–6*). In situ oceanographic data rarely have been collected in the Ross Sea before this time of year because heavy sea ice cover prevents ship access to the polynya during austral spring (October through December). In this report, we use data from the CZCS and the scanning multi-channel microwave radiometer (SMMR) to evaluate distributions of algal pigments and sea ice in the western Ross Sea and the Ross Sea polynya.

We processed a time series of six CZCS images (see the legend of Fig. 2) of phytoplankton pigment and sea ice distribution (using the 750-nm channel) within the western Ross Sea (Table 1), which were obtained during the austral spring and summer of 1978–79 between 10 December and 19 February. Lower resolution (30-km) images of sea ice cover from the SMMR also were processed (*7*) for the Southern Ocean for 1978–79. The Ross Sea polynya was first visible in SMMR imagery on 25 November 1978 and continued to increase in size until 6 January 1979 when it became contiguous with the rest of the Ross Sea.

The earliest springtime CZCS image (10 December) revealed the presence of an intense phytoplankton bloom located south of 75°S. Pigment concentrations estimated at 10 to 40 mg m^{-3} covered an area of ~106,000 km^2 (Fig. 2A). By 23 December, the western margin of annual sea ice had receded westward and a dense phytoplankton bloom had developed near the retreating ice edge between 73° and 75°S, increasing the size of the high-pigment (≥10 mg m^{-3}) region to >126,000 km^2 (Fig. 2B).

The CZCS image for 5 January (Fig. 2C), although contaminated by clouds, revealed that the area of high pigments had diminished substantially and that the phytoplankton bloom was in a state of decline. By 16 January, pigment concentrations over much of the region had dropped to 0.2 to 2.0 mg m^{-3} (Fig. 2D). The most coherent bloom was located in Terra Nova Bay (75°S, 166°E), where pigment concentrations ≥10 mg m^{-3} covered an area of >8000 km^2. Patches of enhanced pigments (1.0 to 12 mg m^{-3}) were also apparent south of 76°S. The 25 January image (Fig. 2E) was similar to that of 16 January, except that the bloom in Terra Nova Bay was more extensive (~16,000 km^2).

By 19 February, the phytoplankton bloom in the western Ross Sea had declined further, both in area and in pigment concentration (Fig. 2F). Pigments over most of the western Ross Sea were reduced to <1 mg m^{-3}. Only near the western coast and along the Ross Ice Shelf were pigment concentrations greater than 2 mg m^{-3}.

The distribution and magnitude of pigments shown in images from 16 January and later agree well with the results of field studies undertaken at the same time of year (*4–6*). Like the CZCS studies, these studies observed waters with low chlorophyll a content north of 75°S and pigment concentrations ranging from 2 to 7 mg m^{-3} southward to the Ross Ice Shelf. This agreement, along with results from validation studies of CZCS for the Southern Ocean (*8*), strongly imply that our estimates of pigment concentration in the Ross Sea are reliable.

Table 1. Seasonal change in CZCS-derived pigment concentration and primary production in the western Ross Sea. Primary production was calculated for each valid pixel according to the regression model of Eppley *et al.* (*12*) and averaged for the full scenes shown in Fig. 2. This model is based on an empirical relation between the mean pigment concentration in the top optical depth and the rate of primary production in situ. It does not require knowledge of the euphotic or mixed layer depth. Rates of primary productivity calculated by this regression, which includes data from the Arctic Ocean and the Southern Ocean, show good agreement with in situ rates of primary production in the western Ross Sea. For example, in situ studies of waters containing 1.5 to 8.2 mg of chlorophyll a per cubic meter measured an average primary productivity rate of 1.4 g of carbon per square meter per day, with values approaching 2 g of carbon per square meter per day (*5*). At similar pigment concentrations, the method of Eppley *et al.* (*12*) yields a production rate of 1.2 to 2.8 g of carbon per square meter per day.

Date	Mean pigment (mg m^{-3} ± SD)	Cloud-free pixels (%)	Pixels >10 mg m^{-3} (%)	Mean production (g C m^{-2} day^{-1} ± SD)
10 Dec. 1978	22.6 ± 19.3	75.9	61.0	3.90 ± 2.72
25 Dec. 1978	12.7 ± 17.1	66.5	36.7	2.54 ± 2.50
5 Jan. 1979	12.5 ± 16.0	34.2	40.4	2.66 ± 2.34
16 Jan. 1979	1.65 ± 3.24	84.7	1.14	0.99 ± 0.82
25 Jan. 1979	3.57 ± 7.45	82.1	12.2	1.32 ± 1.35
19 Feb. 1979	4.07 ± 11.0	46.1	10.5	1.19 ± 1.63
Spring-summer production (10 Dec. to 19 Feb.)				141 g C m^{-2}

National Aeronautics and Space Administration, Goddard Space Flight Center, Greenbelt, MD 20771, USA.

*To whom correspondence should be addressed.

The development of an intense phytoplankton bloom by early December may be the typical pattern for the western Ross Sea. In December 1977, a bloom of *Phaeocystis* sp. extended for 620 km along the Ross Ice Shelf and for 185 km seaward, although concentrations of chlorophyll a were lower (1 mg m^{-3}) than in 1978 (*1*). CZCS images from December 1981, the only other year for which CZCS data are available for this region in spring, exhibit pigment patterns strikingly similar to those from 1978. Moreover, blooms of *Phaeocystis* sp. are regularly advected into McMurdo Sound in December (*9*). On the basis of CZCS pigment fields and reported patterns of ocean circulation (*10, 11*), phytoplankton blooms advected into McMurdo Sound most likely originated in the western Ross Sea in early December.

Rates of primary production calculated (*12*) from the CZCS pigment concentrations were highest for 10 December and averaged 3.9 g of carbon per square meter per day (Table 1). Primary productivity declined steadily thereafter, to <1 g m^{-2} day^{-1} by 16 January and remained relatively constant through 19 February. Integrated primary production between 10 December and 19 February was 141 g m^{-2}, more than 70% of which occurred before mid-January. This value is considerably higher than the 16 g m^{-2} $year^{-1}$ (*13*) and 50 g m^{-2} $year^{-1}$ (*14*) estimated for the open and ice edge zones of the Southern Ocean, respectively, and more than three times the earlier estimate of 45.6 g m^{-2} $year^{-1}$ for the Ross Sea (*15*).

The disparity between our seasonal production estimate and previous reports for the Ross Sea is easily understood when we consider that early estimates of production were based on field measurements made after mid-January, when the bloom may have been in decline. We estimate that primary productivity on 16 January was only 25% of the peak rate, which occurred at least 30 days earlier. Moreover, our value of 141 g m^{-2} may underestimate the spring-summer primary production because it does not include the carbon fixed between 25 November, the date the polynya was first observed by SMMR, and 10 December, the date of the earliest CZCS composite. Assuming, conservatively, that pigments increased exponentially from a winter minimum of 0.05 mg m^{-3} in late November to ~10 mg m^{-3} observed on 10 December (Fig. 2A), we calculate that an additional 30 g m^{-2} would have been fixed, bringing the total spring-summer phytoplankton production to 171 g m^{-2}.

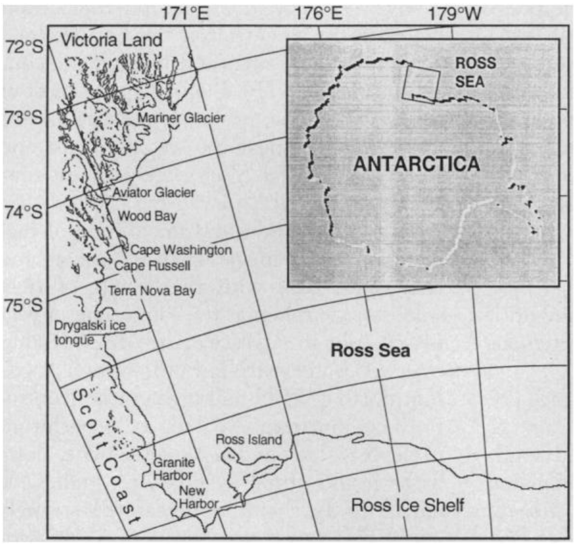

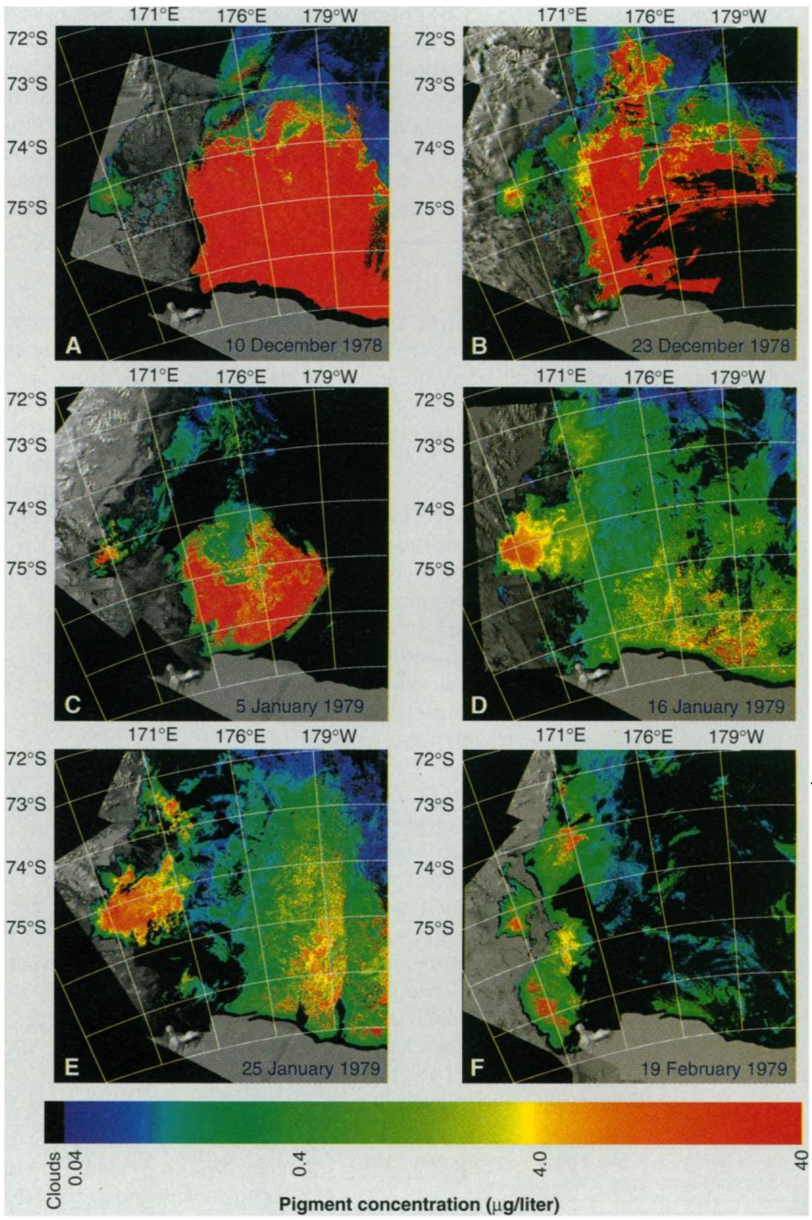

Fig. 1 (left). Detail map of the western Ross Sea showing the permanent (Victoria Land coast, Ross Island) and semipermanent (Ross Ice Shelf, Drygalski ice tongue) features that mark the southern and western boundaries of the study area. **Fig. 2 (right).** Composited CZCS images of sea ice distribution and pigment abundance for **(A)** 10 December 1978, **(B)** 23 December 1978, **(C)** 5 January 1979, **(D)** 16 January 1979, **(E)** 25 January 1979, and **(F)** 19 February 1979. Clouds have been removed so that they are not confused with sea ice, shown here as gray features located north and east of the western Ross Sea boundaries (see Fig. 1). We processed the images with SEAPAK software (*16*), using recently improved cloud and sea ice masks (*17*). The sensor overshoot mask was applied according to (*18*). We computed pigment concentrations using the standard CZCS algorithm (*19*) but with coefficients determined specifically for the Southern Ocean (*8, 20*).

The CZCS data demonstrate that phytoplankton in the western Ross Sea can bloom early, with great intensity, and persist for a long time under conditions that produce and sustain the Ross Sea polynya. Estimates of annual productivity in the western Ross Sea should be revised upward; hence, the relative importance of this region as a CO_2 sink may be greater than previously recognized. It is unfortunate that the CZCS did not provide imagery of the 1978–79 spring phytoplankton bloom earlier than 10 December so that early bloom dynamics could have been monitored. Future satellite ocean color missions, such as the sea-viewing wide field-of-view sensor (SeaWiFS) and the moderate-resolution imaging spectrometer (MODIS), should alleviate this problem by providing data at much finer temporal resolution.

REFERENCES AND NOTES

1. S. Z. El-Sayed *et al.*, *Deep-Sea Res.* **30**, 871 (1983).
2. D. C. Biggs *et al.*, in *Antarctic Nutrient Cycles and Food Webs*, W. R. Siegfried *et al.*, Eds. (Springer-Verlag, Berlin, 1985), pp. 93–103.
3. D. C. Biggs *et al.*, *Tex. A&M Univ. Org. Res. 85-6-T* (Department of Oceanography, Texas A&M University, College Station, 1985).
4. D. L. Wilson *et al.*, *Deep-Sea Res.* **33**, 1375 (1986).
5. W. O. Smith Jr., *et al.*, *Antarct. J. U.S.* **25**, 179 (1990).
6. D. J. Demaster *et al.*, *Oceanography* **5**, 146 (1992).
7. J. C. Comiso and C. W. Sullivan, *J. Geophys. Res.* **91**, 9663 (1986).
8. C. W. Sullivan, K. R. Arrigo, C. R. McClain, J. C. Comiso, J. Firestone, *Science* **262**, 1832 (1993).
9. A. C. Palmisano *et al.*, *J. Plankton Res.* **8**, 891 (1986).
10. J. P. Barry, *Polar Biol.* **8**, 377 (1988).
11. ——— and P. K. Dayton, *ibid.*, p. 367.
12. R. W. Eppley *et al.*, *J. Plankton Res.* **7**, 57 (1985).
13. O. Holm-Hansen *et al.*, in *Adaptations Within Antarctic Ecosystems*, G. A. Llano, Ed. (Smithsonian Institution, Washington DC, 1977), pp. 11–50.
14. W. O. Smith Jr. and D. M. Nelson, *Limnol. Oceanogr.* **35**, 809 (1990).
15. ———, *BioScience* **26**, 251 (1986).
16. C. R. McClain *et al.*, *NASA TM 100728* [National Aeronautics and Space Administration (NASA) Goddard Space Flight Center, Greenbelt, MD, 1991].
17. K. R. Arrigo and C. R. McClain, *NASA TM 104566* (NASA Goddard Space Flight Center, Greenbelt, MD, 1994), vol. 32.
18. J. L. Mueller, *Appl. Opt.* **27**, 438 (1988).
19. H. R. Gordon *et al.*, *ibid.* **22**, 20 (1983).
20. B. G. Mitchell and O. Holm-Hansen, *Deep-Sea Res.* **38**, 1009 (1991).
21. We thank B. Schieber and G. Fu for assistance with image processing, O. Holm-Hansen and D. Biggs for helpful discussions and advice, and M. Lizotte, C. Brown, and L. Harding for editorial comments. Supported by NASA grants 5024 and RTOP 579-11-01-01.

11 April 1994; accepted 14 July 1994

Coupled Land-Ocean-Atmosphere Processes and South Asian Monsoon Variability

Gerald A. Meehl

Results from a global coupled ocean-atmosphere climate model and a model with specified tropical convective heating anomalies show that the South Asian monsoon was an active part of the tropical biennial oscillation (TBO). Convective heating anomalies over Africa and the western Pacific Ocean associated with the TBO altered the simulated pattern of atmospheric circulation for the Northern Hemisphere winter mid-latitude over Asia. This alteration in the mid-latitude circulation maintained temperature anomalies over South Asia through winter and helped set up the land-sea temperature contrast for subsequent monsoon development. South Asian snow cover contributed to monsoon strength but was symptomatic of the larger scale alteration in the mid-latitude atmospheric circulation pattern.

Coupled climate interactions between the ocean and atmosphere contribute to a mechanism that produces biennial variability (TBO) in the troposphere and upper ocean in the tropical Indian and Pacific ocean regions (*1*, *2*). The notion of such coupling has been central to studies of tropospheric biennial oscillations (*3*), and several researchers have linked the biennial component of variability to El Niño–Southern Oscillation (ENSO) (*4–7*). The TBO is associated with modulations of the seasonal cycle, with maxima in the TBO manifested as warm (El Niño) and cold (La Niña) extremes in the tropical Pacific, modulations that have connections to the Indian monsoon (*1*). A biennial component of tropospheric variability is seen in the tropical Pacific and Indian regions in sea-surface temperature (SST) and surface wind (*8–12*), and in the western Pacific, in ocean dynamics (*13–15*). A possible association between the stratospheric quasi-biennial oscillation (QBO) of zonal wind and interannual variability in the tropical troposphere has also been suggested (*16*, *17*). The focus of this report is the extent to which the South Asian monsoon is involved as an active or passive participant in the TBO (and, by extension, ENSO) and the mechanisms by which this interaction occurs.

National Center for Atmospheric Research, Post Office Box 3000, Boulder, CO 80307–3000, USA.

The land-sea temperature contrast is the basic forcing of the South Asian monsoon (of which the Indian monsoon is an integral part) (*18*). More accurately, there is a meridional temperature gradient extending from the tropical Indian Ocean north to the Asian land mass that develops through a considerable depth of the troposphere because South Asia heats more quickly than does the Indian Ocean in spring. Heated air over land rises and draws moist, low-level maritime air inland, where convection and heavy precipitation occur during northern summer to fuel the monsoon circulation further. Such land-sea temperature contrasts are important in other tropical rainfall regimes (*19*) as well as for the simulation of monsoon rainfall in various general circulation models (GCMs) (*20*) and in paleoclimate studies (*21*). Consequently, the South Asian monsoon could be actively involved in the TBO and ENSO through modulations of temperature contrast between South Asian land areas and the Indian Ocean.

Links between the South Asian monsoon and the Southern Oscillation have also been shown to have a biennial tendency (*22–25*). Additionally, snow cover may alter land-surface temperature and subsequent monsoon strength, as suggested in the late 1800s (*26*). Years with enhanced winter and spring snow cover over South Asia tend to have below-normal monsoon rainfall (*27–30*). Consequently, tropical–mid-latitude interaction has also been proposed as playing some role in monsoon evolution (*24*).

The National Center for Atmospheric Research's (NCAR's) coarse-grid, global coupled ocean-atmosphere GCM (*31*) was used to study the processes postulated above. This type of model is a useful tool for elucidating basic processes in the coupled climate system. It can represent aspects of the observed large-scale mean climate (*31*), climate variability compared to satellite observations (*32*), and some elements of ENSO-related variability (*33*). Because there are no correction terms used to force the coupled model to the observed state, the model-simulated SSTs in the tropics tend to be too cool, thus enhancing land-sea temperature contrast in the monsoon region. Yet, the pattern of mean monsoon seasonal precipitation and the variability of the simulated South Asian monsoon has been shown to be comparable to the observed pattern (*34*).

The atmospheric model had an approximate horizontal resolution of 4.5° latitude and 7.5° longitude with nine vertical levels. Soil moisture was parameterized by a simple reservoir formulation, and clouds, precipitation, snowfall, and resulting snow cover were computed. The global dynamical ocean model had a resolution of 5° by 5°